Contrib Mineral Petrol (2006) 152: 1–17
DOI 10.1007/s00410-006-0085-4

ORIGINAL PAPER

John Adam · Trevor Green

Trace element partitioning between mica- and amphibole-bearing garnet lherzolite and hydrous basanitic melt: 1. Experimental results and the investigation of controls on partitioning behaviour

Received: 15 June 2005 / Accepted: 8 March 2006 / Published online: 13 May 2006

Abstract Thirty five minor and trace elements (Li, Be, B, Sc, Cu, Zn, Ga, Ge, As, Rb, Nb, Mo, Ag, Cd, In, Sn, Sb, Cs, Ba, La, Ce, Nd, Sm, Tb, Ho, Tm, Lu, Hf, Ta, W, Tl, Pb, Bi, Th and U) in experimentally produced near-liquidus phases, from a primitive nelpheline basanite from Bow Hill in Tasmania (Australia), were analysed by LAM ICP-MS. A number of halogens (F, Cl and I) were also analysed by electron microprobe. The analyses were used to determine mineral/melt partition coefficients for mica, amphibole, garnet, clinopyroxene, orthopyroxene and olivine for conditions close to multiple saturation of the basanite liquidus with garnet lherzolite (approximately 2.6 GPa and 1,200°C with 7.5 wt% of added H_2O). A broader range of conditions was also investigated from 1.0 GPa and 1,025°C to 3.5 GPa and 1,190°C with 5–10 wt% of added H_2O. The scope and comprehensiveness of the data allow them to be used for two purposes, these include the following: an investigation of some of the controlling influences on partition coefficients; and the compilation of a set partition coefficients that are directly relevant to the formation of the Bow Hill basanite magma by partial melting of mantle peridotite. Considering clinopyroxene, the mineral phase for which the most data were obtained, systematic correlations were found between pressure and temperature, mineral composition, cation radius and valence, and ΔG^{coulb} (the coulombic potential energy produced by substituting a cation of mismatched valence into a crystallographic site). ΔG^{coulb} is distinctly different for different crystallographic sites, including the M2 and M1 sites in clinopyroxene. These differences can be modelled as a function of variations in optimum valence (expressed as 1 sigma standard deviations) within individual M1 and M2 site populations.

Communicated by B. Collins

J. Adam · T. Green
ARC National Key Centre for the Geochemical Evolution and Metallogeny of Continents, Department of Earth and Planetary Sciences, Macquarie University, Sydney, NSW 2109, Australia

J. Adam (✉)
408 Princes Highway, Blakehurst, NSW 2221, Australia
E-mail: john_adam@bigpond.com
Tel.: +61-2-95463140

Introduction

Experimental data on minor and trace element partitioning between minerals and melts are often of limited usefulness for interpreting natural igneous systems. This is because partition coefficients [D_i = (concentration of element i in mineral)/(concentration of element i in melt)] are influenced by so many different factors, including pressure, temperature, mineral composition and melt composition, that they are difficult to accurately predict for changed circumstances. This is in spite of many efforts at rationalizing the way different factors affect partition coefficients (e.g. Onuma et al. 1968; Brice 1975; Nielsen 1985; Blundy and Wood 1991, 1994; Gaetani and Grove 1995; Schosnig and Hoffer 1998; Hill et al. 2000). Thus, unless data are either deliberately obtained or fortuitously available for the specific circumstances being investigated, it is difficult to know exactly how elements will partition. In this paper, we examine this problem for the case of a nepheline basanite (UT-70489) from Bow Hill in Tasmania, Australia. The basanite has primitive geochemical characteristics (12.0 wt% MgO, 380 ppm Ni, and Mg no. = 64.6) that are consistent with the original magma being close to an unmodified product of partial melting of mantle peridotite. Its near-liquidus phase relationships were investigated by Adam (1989, 1990) who determined conditions of multiple saturation with garnet lherzolite at about 2.6 GPa and 1,200°C with 4.5 wt% H_2O and 2.0 wt% CO_2 dissolved in the basanite melt.

This study was used to investigate the partitioning of minor and trace elements between the Bow Hill basanite magma and residual garnet lherzolite phases including mica, amphibole, garnet, clinopyroxene, orthopyroxene and olivine. A combination of electron microprobe and LAM ICP-MS (laser ablation microprobe and inductively-coupled plasma mass spectrometry) was used to analyse major, minor and trace elements in experimentally produced near-liquidus phases. As far as was possible partition coefficients were obtained for conditions close to those of multiple saturation with garnet lherzolite. But a broader range of conditions, from 1.0 GPa and 1,025°C to 3.5 GPa and 1,190°C, was also examined. Because of the size and scope of the resulting data set, it was possible to separately examine the effects of pressure, temperature, lattice-strain, cation valence, mineral chemistry and H_2O concentration on partition coefficients. The results of this investigation are reported in this paper. The use of the partition coefficients to study melting behaviour and the nature of the basanite magma's source is the subject of a separate paper.

Experimental and analytical procedures

Starting composition

The starting composition used in experiments was based on a powdered sample of the natural rock. This was doped with a total of 39 trace elements including Li, Be, B, Sc, Cu, Zn, Ga, Ge, As, Rb, Nb, Mo, Ag, Cd, In, Sn, Sb, Cs, Ba, La, Ce, Nd, Sm, Tb, Ho, Tm, Lu, Hf, Ta, W, Tl, Pb, Bi, Th, U, F, Cl, Br and I. The concentrations of non-volatile dopants varied from about 100 to 1000 ppm to give a total of 1.4 wt% of added trace oxides. Excepting Be all of the non-volatile dopants were added to the starting mix in aqueous solutions (as either chlorides or nitrates). Because of its dangerous toxicity, Be was added as natural beryl (to avoid the handling of H_2O-soluble Be). After being dried and thoroughly ground the doped mix was melted in a vertical furnace and then quenched in water to form a glass. This was done twice. Because of the volatility of some of the dopants (particularly Sn, Sb, Mo, In and Tl) the melting time was kept to a minimum (about 30 s). A total of 2,000 ppm F was added to the dried and powdered glass as FeF_3. Cl, Br and I were added to individual experiments (along with H_2O) in an aqueous solution containing 10,000 ppm of each halide (present as potassium halides). Most of the experiments contained 7.5 wt% H_2O and thus ideally should also have had 750 ppm each of Cl, Br and I. In practice concentrations of both F and Cl were higher than originally intended with ~0.24 wt% F and from 0.45 to 0.99 wt% Cl being present in some runs. This was due to a combination of F and Cl present in the original rock, the use of Cl-bearing aqueous solutions (ICP-MS analytical standards) as a source of dopants, and the short melting times required to preserve volatile dopants such as Mo, Sb and Sn. The results of previous experiments on halogen-enriched and halogen-free basanite compositions (see Adam et al. 1993) show that these enrichments would not perceptibly affect the partition coefficients of other (non-volatile) elements.

Experimental procedures

All experiments were conducted in piston–cylinder apparatus of the type described by Boyd and England (1960) using a piston-in technique. A minus 10% correction for friction was made to measured pressures (Green et al. 1966). Furnace assemblies were of 12.7 mm diameter and made of graphite with composite talc and pyrex® sleeves and boron-nitride inserts. Temperatures were measured using $Pt–Pt_{90}Rh_{10}$ thermocouples and automatically regulated by an Electromax V single loop controller.

Samples were loaded into graphite inner capsules contained in Pt outer capsules, instead of the single $Ag_{50}Pd_{50}$ capsules originally used by Adam (1989, 1990). This was done because earlier experiments had shown that Cu, Mo, Sb, Cr and Ni alloy with $Ag_{50}Pd_{50}$, $Au_{80}Pd_{20}$ and Pt so readily that it is impossible to maintain a constant bulk composition unless the starting material is isolated from the precious metal capsules by graphite. Both H_2O and dissolved halides were added first with a graduated microsyringe. Powdered sample was added on top of this to give a total sample mass of 15 mg. The concentration of H_2O added was in most cases 7.5 wt%. This quantity was intended to replicate the liquidus temperatures achieved by Adam (1989, 1990) who used 4.5 wt% H_2O and 2.0 wt% CO_2. We did not add CO_2 in case reaction with the graphite capsules caused its concentration to vary during runs. Once loaded the graphite capsules were fitted with lids and placed inside the Pt outer capsules. The Pt capsules were then welded closed with an electric-arc welder. During welding capsules were kept frozen in a liquid nitrogen bath. If this wasn't done conduction of the electric current through the halide solutions in capsules caused vaporization of added H_2O. In order to promote the growth of large crystals run temperatures were initially taken to 110°C above target run temperatures. After 30 min, temperatures were gradually reduced over a further 30 min to final run temperatures. Total run times were 48 h. After each experiment capsules were longitudinally sectioned, mounted in epoxy and polished using non-aqueous lubricants.

Of the near-liquidus phases previously crystallized from UT-70489 garnet was the most difficult to duplicate in the present experiments. This was probably the result of changes to both the experimental procedures and starting composition originally used to grow garnet. Because of these differences fO_2, Fe^{+3} and Al_2O_3 would all have been greater in the original experiments. Both Adam and Green (1994) and Green and Pearson (1985) found that pyroxenes produced under oxidizing (i.e.

haematite–magnetite buffered) conditions are relatively Al_2O_3 enriched. If this is due to high fO_2 increasing the relative activity of Al_2O_3 low fO_2 might be expected to have the reverse effect and therefore destabilize garnet. Our use of a temperature over-step when beginning experiments would also have inhibited the nucleation of garnet. To overcome these retarding factors we added 2.0 wt% of Al_2O_3 to the starting composition for two experiments. These were run in unlined $Au_{80}Pd_{20}$ capsules with 10 wt% of added H_2O and used to grow garnet at 1,180 and 1,190°C and 3.5 GPa.

Analytical methods

Major and minor elements, including halogens, were analysed with a Cameca® SX50 electron microprobe. Corrections to the raw data were made with the PAP program of Pouchu and Pichoir (1984). The accelerating voltage was 15 kV at a current of 20 nA. Counting times were 10 s for peaks and 5 s for each background. For minerals a beam diameter of 1 μm was used. This was increased to 30 μm for the analysis of quenched melt areas. To minimize the loss of Na and K during analyses these elements were analysed first during each analytical cycle. In spite of this losses of from 0.0 to 2.0 wt% Na_2O and 0.0 to 0.5 wt% K_2O are estimated for analyses of quenched melts. The standards used were albite, orthoclase, kyanite, wollastonite, rutile, olivine, Mn-garnet, topaz and apatite.

Trace elements and some minor elements were analysed with a laser microprobe coupled to an Argilent 7500S ICP-MS. Samples were ablated with a 30 μm diameter beam of UV light (λ = 266 nm) from a Continuum Surelite I-20 Q-switched Nd:YAG laser. Procedures were similar to those used by Norman et al. (1996) but used a mixture of He and Ar to optimize ablation characteristics and detection limits. The energy per pulse was kept at 0.2 mJ at a frequency of 4 Hz. Higher energies caused excessive fragmentation of the fragile sample materials. For amphiboles, clinopyroxenes and garnets CaO was the internal standard used to calibrate ICP-MS analyses. For olivine and orthopyroxene MgO was used instead instead of CaO, but for mica Al_2O_3 was used. In each case, electron microprobe analyses of CaO, MgO and Al_2O_3 were chosen from points close to the spots analysed by ICP-MS. Typically from three to five analyses were made of each phase produced by an experiment.

Minimum detection limits (99% confidence) for crystals and quenched melts were: 0.01–0.1 ppm for Sc, V, Co, Ga, In, Rb, Cs, Sr, Y, Zr, Nb, Ta, Mo, Ag, W, Tl, Pb, Bi, Sb, REE, Th and U; 0.1 to 1.0 ppm for Li, Be, Cr, Ge, Ni, Cu, Zn, As, Cd, Sn, Hf and Ba; and 1—5 ppm for B, P, Ti, Al and Mg. The precision of individual analyses varied depending upon a number of factors; these included the element and isotope analysed, and the sample's size and homogeneity. In the case of individual isotopes, 1 sigma errors were normally larger for high concentrations than they were for low concentrations. Thus, they were usually smaller for analyses of crystals than for quenched melts. The 1 sigma errors calculated from variations in replicate analyses of crystals and glasses were typically several times larger than the fully integrated 1 sigma errors determined from counting statistics.

Experimental results

General description

A list of runs, run product modes and experimental conditions is given in Table 1. The degree of crystallization in runs varies from 38 to 9%. Generally crystals accumulated in the lower parts of capsules. Their size and degree of intergrowth with other phases varies from run to run. All runs produced clinopyroxene as well as quenched melt. Depending upon run conditions, the quenched melt forms either a brown glass or a felted mass of fine crystals, with glass present in some cases. Clinopyroxene usually forms olive-green blocky crystals

Table 1 Run conditions and run products from experiments on the nepheline basanite UT-70489

Run	°C	GPa	% H_2O	Run product modes (wt%)								
				Garnet	cpx	opx	Olivine	Mica	amph	Apatite	Fe loss	Melt
1951	1,025	1.0	7.5		4		9		18	0.1		68.9
R79	1,075	1.0	5		4		10					86
1950	1,050	2.0	10		9	1		7	17			66
R77	1,100	2.0	10		6		3					91
R78	1,100	2.5	10		13			3.7			1	82.3
1948	1,160	2.5	7.5		10.6	1					0.4	88
1949	1,160	2.7	7.5		18	2		3.5			2	74.5
R80	1,170	3.0	7.5		17.4	4					2.6	76
1956	1,180	3.5	10	23	12						3	62
1955	1,190	3.5	10	13	7						5	75

Run product modes are from mass balances for major and minor elements in run products and starting compositions. % H_2O is the weight percent of H_2O added to starting compositions

Table 2 Electron microprobe analyses of major and minor elements in run products and the anhydrous starting composition

Run	1,190°C	3.5 GPa	1,180°C	3.5 GPa	1,170°C	3.0 GPa	1,160°C	2.7 GPa	1,160°C	2.5 GPa	1,100°C	2.5 GPa	1,100°C	2.0 GPa	1,050°C	2.0 GPa	1,075°C	1.0 GPa	1,025°C	1.0 GPa
	1955		1956		R80		1949		1948		R78		R77		1950		R79		1951	
	cpx	1σ	cpx	1σ	cpx	1σ	cpx	1σ	cpx	1σ	cpx	1σ	cpx	1σ	cpx	1σ	cpx	1σ	cpx	1σ
	av.	$n = 5$	av.	$n = 9$	av.	$n = 12$	av.	$n = 6$	av.	$n = 9$	av.	$n = 11$	av.	$n = 6$	av.	$n = 5$	av.	$n = 7$	av.	$n = 2$
SiO_2	52.98	0.29	53.65	0.50	52.53	0.64	52.53	0.93	52.99	0.78	52.50	0.50	52.57	0.65	52.89	0.27	51.80	1.49	50.66	1.47
TiO_2	0.41	0.05	0.57	0.14	0.61	0.20	0.74	0.29	0.58	0.16	0.58	0.16	0.70	0.15	0.55	0.11	1.20	0.37	1.33	0.59
Al_2O_3	4.61	0.44	5.73	1.11	6.88	0.74	6.73	1.25	5.46	0.89	4.33	0.87	3.72	0.62	3.19	0.51	3.70	1.21	3.64	1.43
Cr_2O_3	0.03	0.03	0.07	0.02	0.23	0.06	0.21	0.04	0.27	0.09	0.24	0.05	0.27	0.09	0.18	0.05	0.90	0.34	0.54	0.12
FeO	4.38	0.59	4.54	0.86	6.28	0.67	6.65	0.46	6.19	0.63	6.11	0.51	5.72	0.37	6.82	0.27	5.39	0.29	5.82	0.25
MnO	0.08	0.03	0.10	0.03	0.17	0.01	0.17	0.03	0.15	0.02	0.16	0.02	0.16	0.01	0.16	0.02	0.11	0.03	0.11	0.03
NiO	0.01	0.01	0.04	0.03	0.04	0.04	0.05	0.03	0.03	0.02	0.03	0.03	0.04	0.01	0.02	0.01	0.02	0.02	0.01	0.01
MgO	15.51	0.39	14.91	0.82	16.49	0.68	16.18	0.75	17.24	0.63	17.02	0.88	16.81	0.33	16.25	0.41	15.38	0.88	14.69	0.99
CaO	18.05	0.47	16.74	0.60	14.21	0.91	15.30	0.64	16.02	1.06	17.32	0.73	19.26	0.52	18.62	0.44	21.44	0.39	21.62	0.03
Na_2O	2.02	0.12	2.69	0.52	1.88	0.09	1.67	0.15	1.33	0.10	1.14	0.17	0.79	0.09	0.86	0.07	0.61	0.09	0.62	0.06
K_2O	0.01	0.01	0.01		0.00		0.01	0.01	0.01		0.01	0.02	0.02	0.03	0.01		0.02	0.03	0.01	0.01
P_2O_5	0.04	0.01	0.04	0.02	0.03	0.02	0.03	0.03	0.03	0.02	0.04	0.03	0.04	0.02	0.01	0.02	0.02	0.02	0.08	0.06
Total	98.12		99.09		99.35		100.27		100.30		99.48		100.10		99.56		100.59		99.13	
Mg no.	86.3		85.4		82.4		81.3		83.2		83.2		84.0		80.9		83.6		81.8	

Run	1,170°C	3.0 GPa	1,160°C	2.7 GPa	1,160°C	2.5 GPa	1,050°C	2.0 GPa		1,100°C	2.0 GPa	1,075°C	1.0 GPa	1,025°C	1.0 GPa		1,190°C	3.5 GPa	1,180°C	3.5 GPa
	R80		1949		1948		1950			R77		R79		1951			1955		1956	
	opx	1σ	opx	1σ	opx	1σ	opx	1σ		Olivine	1σ	Olivine	1σ	Olivine	1σ		Garnet	1σ	Garnet	1σ
	av.	$n = 3$	av.	$n = 5$	av.	$n = 4$	av.	$n = 3$		av.	$n = 10$	av.	$n = 5$	av.	$n = 3$		av.	$n = 10$	av.	$n = 9$
SiO_2	54.96	0.24	54.43	0.50	55.13	0.28	54.35	0.28		39.64	0.24	39.73	0.12	38.65	0.18		41.15	0.15	41.08	0.15
TiO_2	0.18	0.01	0.24	0.04	0.22	0.02	0.27	0.00		0.02	0.01	0.03	0.01	0.05	0.00		0.47	0.03	0.51	0.03
Al_2O_3	3.60	0.19	4.74	0.88	3.25	0.15	2.24	0.08		0.02	0.01	0.03	0.01	0.03	0.02		22.35	0.31	22.50	0.31
Cr_2O_3	0.16	0.02	0.20	0.03	0.18	0.01	0.12	0.00		0.03	0.02	0.04	0.03	0.03	0.01		0.31	0.05	0.13	0.05
FeO	9.72	0.38	9.97	0.32	9.55	0.37	12.60	0.23		17.98	0.26	20.13	0.28	21.05	0.51		9.71	0.73	11.56	0.73
MnO	0.18	0.02	0.17	0.03	0.16	0.01	0.20	0.00		0.20	0.02	0.26	0.02	0.27	0.01		0.33	0.02	0.34	0.02
NiO	0.02	0.03	0.01	0.02	0.02	0.01	0.04	0.02		0.09	0.03	0.11	0.03	0.21	0.04		0.02	0.01	0.01	0.01
MgO	29.47	0.12	29.11	0.36	30.56	0.27	28.21	0.18		43.01	0.29	41.30	0.34	39.16	0.81		17.88	0.85	16.99	0.85
CaO	1.30	0.08	1.35	0.07	1.58	0.16	1.30	0.07		0.13	0.01	0.22	0.02	0.23	0.01		6.77	0.67	6.35	0.67
Na_2O	0.26	0.03	0.25	0.02	0.31	0.18	0.17	0.10		0.01	0.01	0.01	0.00	0.03	0.01		0.06	0.01	0.09	0.01
K_2O	0.00		0.00		0.01	0.01	0.01	0.00		0.00		0.00		0.01	0.00		0.00		0.00	
P_2O_5	0.00		0.02	0.03	0.01	0.01	0.02	0.03		0.06	0.02	0.08	0.03	0.11	0.02		0.05	0.03	0.07	0.03
Total	99.85		100.49		100.98		99.53			101.19		101.94		99.83			99.10		99.62	
Mg no.	84.4		83.9		85.1		80.0			81.0		78.5		76.8			76.6		72.4	

Run	1,160°C	2.7 GPa	1,100°C	2.5 GPa	1,050°C	2.0 GPa		1,050°C	2.0 GPa	1,025°C	1.0 GPa		1,025°C	1.0 GPa	UT-70489[a]
	1949		R78		1950			1950		1951			1951		
	Mica	1σ	Mica	1σ	Mica	1σ		amph	1σ	amph	1σ		Apatite		
	av.	$n = 5$	av.	$n = 6$	av.	$n = 5$		av.	$n = 5$	av.	$n = 5$		$n = 1$		
SiO_2	38.56	0.37	38.81	0.59	38.91	0.63		44.51	0.48	42.22	0.31		0.55		43.88
TiO_2	2.26	0.07	1.89	0.09	2.26	0.11		2.01	0.14	3.42	0.24		0.04		2.32
Al_2O_3	15.78	0.24	15.03	0.24	14.79	0.56		11.32	0.31	11.34	0.28		0.02		11.35

Table 2 (Contd.)

Run	1,160°C	2.7 GPa	1,100°C	2.5 GPa	1,050°C	2.0 GPa	1,050°C	2.0 GPa	1,025°C	1.0 GPa	1,025°C	1.0 GPa	UT-70489[a]
	1949		R78		1950		1950		1951		1951		
	Mica	1σ	Mica	1σ	Mica	1σ	amph	1σ	amph	1σ	Apatite		
	av.	*n* = 5	av.	*n* = 6	av.	*n* = 5	av.	*n* = 5	av.	*n* = 5	*n* = 1		
Cr_2O_3	0.10	0.03	0.16	0.03	0.15	0.07	0.18	0.06	0.38	0.20	0.01		0.06
FeO	6.96	0.06	6.75	0.15	7.51	0.46	7.69	0.2	7.55	0.65	0.61		11.71
MnO	0.04	0.02	0.02	0.02	0.03	0.01	0.09	0.01	0.09	0.02	0.06		0.19
NiO	0.13	0.02	0.16	0.01	0.17	0.03	0.07	0.02	0.04	0.01			0.04
MgO	20.64	0.19	21.29	0.38	20.88	0.51	17.22	0.31	15.87	0.41	0.14		12.00
CaO	0.02	0.02	0.01	0.01	0.03	0.02	10.1	0.07	11.31	0.12	51.68		9.36
Na_2O	0.63	0.03	0.71	0.01	0.99	0.02	2.95	0.04	2.66	0.09	0.09		4.12
K_2O	9.45	0.05	8.96	0.09	8.53	0.08	1.3	0.06	1.23	0.13	0.03		2.02
P_2O_5	0.00		0.01	0.01	0.00		0.04	0.02	0.04	0.01	44.63		1.43
F	0.44	0.04	0.36	0.02	0.44	0.05	0.22	0.03	0.35	0.02			
Cl	0.22	0.01	0.15	0.06	0.1	0.01	0.07	0.00	0.08	0.01			
I	0.00	0.01	0.02	0.02	0.03	0.02	0.0	0.00	0.00	0.0			
Total	95.08		94.33		94.82		97.77		96.58		97.86		98.6
Mg no.	84.1		84.9		83.2		80.0		78.9				64.6

Run	1,190°C	3.5 GPa	1,180°C	3.5 GPa	1,170°C	3.0 GPa	1,160°C	2.7 GPa	1,160°C	2.5 GPa	1,100°C	2.5 GPa	1,100°C	2.0 GPa	1,050°C	2.0 GPa	1,075°C	1.0 GPa	1,025°C	1.0 GPa
	1955		1956		R80		1949		1948		R78		R77		1950		R79		1951	
	Matrix	1σ	Matrix	1σ	Matrix	1σ	Matrix	1σ	Matrix	1σ	Matrix	1σ	Matrix	1σ	Matrix	1σ	Matrix	1σ	Glass	1σ
	av.	*n* = 9	av.	*n* = 10	av.	*n* = 7	av.	*n* = 5	av.	*n* = 10	av.	*n* = 5	av.	*n* = 10	av.	*n* = 5	av.	*n* = 9	av.	*n* = 5
SiO_2	41.77	1.13	40.99	1.68	39.59	0.39	39.88	0.31	40.53	0.46	39.26	0.59	40.89	0.51	39.14	0.25	42.55	0.25	41.36	0.17
TiO_2	2.63	0.15	3.57	0.08	2.88	0.03	2.86	0.05	2.68	0.06	2.64	0.04	2.55	0.06	2.76	0.03	2.75	0.04	2.57	0.03
Al_2O_3	11.31	0.31	10.66	0.38	11.71	0.13	11.93	0.05	11.65	0.13	11.33	0.26	11.47	0.18	11.39	0.11	12.37	0.19	12.48	0.06
Cr_2O_3	0.04	0.02	0.01	0.01	0.02	0.01	0.04	0.01	0.03	0.01	0.02	0.01	0.05	0.02	0.02	0.02	0.03	0.01	0.02	0.01
FeO	4.73	0.33	5.95	0.51	8.11	0.21	8.98	0.25	10.22	0.35	9.86	0.2	10.99	0.38	10.27	0.33	9.95	0.05	9.70	0.23
MnO	0.12	0.01	0.13	0.01	0.17	0.02	0.17	0.01	0.17	0.03	0.15	0.01	0.16	0.02	0.19	0.01	0.19	0.02	0.20	0.02
NiO	0.00	0.00	0.01	0.01	0.00	0.01	0.01	0.02	0.01	0.01	0.01	0.00	0.01	0.02	0.01	0.01	0.01	0.02	0.01	0.01
MgO	9.98	1.56	6.76	0.93	8.64	0.44	9.10	0.18	9.60	0.54	9.12	0.68	8.81	0.54	7.48	0.37	6.88	0.10	5.70	0.07
CaO	7.65	1.46	6.87	0.40	8.35	0.38	7.84	0.21	8.06	0.36	6.53	0.77	8.82	0.39	8.13	0.36	9.31	0.03	8.35	0.08
Na_2O	*4.11*		4.70	0.52	*4.00*		3.43	0.11	*3.70*		2.91	0.17	*3.70*		2.92	0.19	3.85	0.02	4.13	0.03
K_2O	2.50	0.71	3.17	0.56	*2.50*		2.28	0.07	2.10	0.18	1.9	0.27	2.06	0.31	1.60	0.19	2.22	0.02	1.97	0.03
P_2O_5	1.65	0.30	2.18	0.16	2.13	0.14	1.78	0.1	1.71	0.10	1.41	0.11	1.62	0.06	1.98	0.1	1.76	0.11	1.65	0.06
F	NA		NA		NA		0.30	0.04	NA		0.27	0.04	NA		0.23	0.02	NA		0.26	0.03
Cl	NA		NA		NA		0.65	0.08	NA		0.53	0.08	NA		0.35	0.04	NA		1.45	0.01
I	NA		NA		NA		0.04	0.04	NA		0.04	0.02	NA		0.02	0.03	NA		0.06	0.01
total	85.00		85.00		81.61		89.28		84.66		85.99		91.13		86.48		91.87		89.91	
Original Na	2.61	0.43			2.94	0.20			3.09	0.23			2.90	0.21	2.80	0.14			3.89	0.05
Original K					2.21	0.22									1.60	0.31			2.03	0.03
est. H_2O	13.3		16.3		9.9		9.9		8.5		12.0		11.0		14.1		5.8		10.3	
Mg no.	79.0		66.9		65.5		63.6		62.6		62.2		58.8		56.5		55.2		51.2	

Figures in italics for Na_2O and K_2O indicate values calculated from mass balances between run products and starting compositions. Original values are those analysed by the electron microprobe. est. H_2O is the H_2O concentration in the melt phase calculated from mass balance between run products and starting composition. Mg no. = 100 Mg/(Mg + total Fe)
NA not analysed, *cpx* clinopyroxene, *opx* orthopyroxene, *amph* amphibole, *av.* average, *n* number of analyses used to compile average, *1σ* 1 sigma standard deviation
[a]XRF analysis of rock used to make starting composition. The glass prepared for experiments includes 1.40 wt% trace oxides

that are sometimes intergrown with other phases. Most experiments produced crystals large enough (with minimum dimensions >50 μm) to be analysed by LAM ICP-MS. Orthopyroxene was characteristic of near-liquidus runs at pressures of 2.5 GPa and above, but it was also produced in one exceptionally hydrous but low temperature run at 2.0 GPa. It occurs as grey–brown anhedral crystals that are usually intergrown with other mineral phases. Its presence in run products is a surprise because in the previous study by Adam (1989, 1990) it was only stabilized after experiments were seeded with orthopyroxene. Evidently orthopyroxene's stability was enhanced by the experimental procedures used in this study. Only one experiment produced orthopyroxene crystals large enough to be successfully analysed by LAM ICP-MS.

Olivine crystallized at pressures less than 2.5 GPa where it replaced orthopyroxene as a near-liquidus phase. It forms colourless crystals of either rounded or blade-like habit. In contrast to orthopyroxene, amphibole's stability was not enhanced in our experiments. In the earlier experiments of Adam (1989, 1990) amphibole and mica were both stable to at least 1,150°C at 2.5 GPa. With the addition of F we expected that amphibole would be a near-liquidus phase at 2.5 GPa. But after a number of attempts it was crystallized only at 2.0 GPa and 1,050°C (with 10.0 wt% of H_2O added instead of 7.5 wt.%) and at 1,025°C and 1.0 GPa with 7.5 wt% H_2O. It forms equant brown crystals up to 200 μm in diameter that are sometimes intergrown with other crystal phases. Although mica was not a near-liquidus phase at 2.5 GPa, it was at 2.7 GPa being produced, together with clinopyroxene and orthopyroxene, at 1,160°C. It was also stable at lower temperatures and pressures crystallizing together with amphibole at 1,050*degr*C and 2.0 GPa. It forms red–brown platy crystals up to 100 μm across that are intergrown with other mineral phases. Garnets from experiments at 3.5 GPa occur as red–brown, euhedral to subhedral crystals up to 200 μm in diameter. They contain variable amounts of included clinopyroxene and glass.

Analytical results

Analyses of major and minor elements in crystals and quenched melts from experiments are given in Table 2. Mineral/melt partition coefficients calculated from LAM ICP-MS analyses are given in Table 3. LAM ICP-MS analyses of individual run products are available from the authors upon request. The precision and accuracy of analyses varied depending upon absolute concentration, crystal size and the presence or absence of other included phases. The effects of even very minor analytical contamination are made obvious by examining data on Onuma diagrams (plots of partition coefficients versus the ionic radii of isovalent cations). Horizontal digressions from parabolic trends usually indicate analytical contamination. Such analyses were not used. For the most incompatible elements, such as Ba, Rb, Cs and W in pyroxenes, olivine and garnet, some degree of contamination seems probable in most analyses. This does not indicate significant degrees of contamination for other elements, only that the partition coefficients for these elements appear to be vanishingly small (< 0.001); this conclusion is consistent with both the lowest measured values and with the detection limits and precision of the LAM ICP-MS analyses.

Another factor may have separately affected partition coefficients. After analyses mass balances were calculated between run products and starting compositions. In some cases, these showed loss of Fe from starting compositions as well as variable losses of Ni, Cr, Cu, Ag, Sn, Cd and Bi. These tended to increase with pressure and temperature. In contrast to these elements, the mass balances for most other elements analysed by LAM ICP-MS were excellent with relative concentrations in bulk run products and starting compositions agreeing to within a few per cent. The problem is one that appears to be characteristic of hydrous experiments conducted in graphite capsules, although not evident in similar but anhydrous experiments. We at first considered it probable that an Fe-alloy precipitate had formed, but a number of factors make this unlikely. Green (1973) produced hydrous basanitic glasses in graphite capsules using similar furnace assemblies, temperatures and pressures to those employed in our experiments. Later FTIR analyses of these glasses (Brey and Green 1975) showed them to contain dissolved carbonate ions produced by reaction between the basanitic melts and graphite capsules. The presence of such an oxidized species is not consistent with conditions reducing enough to produce an Fe-metal precipitate. As well, anhydrous experiments conducted in graphite capsules do not seem to be affected in the same way, although this could be partially accounted for by the higher temperatures generally characteristic of such experiments. In the absence of conditions reducing enough to produce an Fe-alloy, it is possible that the affected elements were incorporated into volatile organometallic compounds and then subsequently lost to either a vapour phase or to the outer Pt capsule. This idea was suggested to us by Greg Yaxley and David Green (personal communication). A final possibility is that the graphite capsules leaked and allowed contact of the melt phase with the Pt outer capsules, but we found no evidence of this. As we also found no separate evidence of a vapour phase, the cause of the material losses during experiments remains a matter of speculation. Whatever the reasons the partition coefficient results for the affected elements are noticeably less consistent than for other elements.

Of the halogens, only F and Cl could be satisfactorily analysed with the electron microprobe in both crystals and melts. This was because they were present in much higher concentrations than either Br or I. Cl in particular was strongly concentrated in some runs and appears to be heterogeneous in the starting mix. This was

Table 3 Mineral/melt partition coefficients calculated from LAM ICP-MS analyses of run products

	Run 1956		Run R80		Run 1949		Run 1948		Run R78		Run R77		Run 1950		Run R79		1949	
°C	1,180		1,170		1,160		1,160		1,100		1,100		1,050		1,075		1,160	
GPa	3.5		3.0		2.7		2.5		2.5		2.0		2.0		1.0		2.7	
	cpx/melt	1σ	cpx/melt	1σ	cpx/melt	1σ	cpx/melt	1σ	cpx/melt	1σ	cpx/melt	1σ	cpx/melt	1σ	cpx/melt	1σ	opx/melt	1σ
Li7	0.270	0.014	0.35	0.07	0.26	0.04	0.23	0.02	0.21	0.02	0.16	0.01	0.17	0.01	0.14	0.01	0.28	0.02
Be9	0.070	0.002	0.09	0.02	0.08	0.02	0.045	0.028	0.06	0.00	0.085	0.010	0.14	0.02	0.1	0.02	0.06	0.02
B10	0.020	0.002	0.033	0.001	0.018	0.000	< 0.005		0.02	0.02	0.03	0.01	0.1	0.01	0.17	0.01	< 0.0003	
Mg25	2.11	0.08	1.76	0.12	1.83	0.19	1.85	0.13	1.76	0.04	2.20	0.12	1.92	0.14	2.14	0.08	3.4	0.12
Al27	0.58	0.03	0.62	0.09	0.57	0.09	0.46	0.03	0.36	0.00	0.33	0.01	0.39	0.02	0.32	0.05	0.43	0.02
P31	0.02	0.002	0.024	0.01	0.017	0.008	0.010	0.005	0.0100	0.0004	0.01	0.00	0.06	0.01	0.018	0.002	0.007	0.002
Ca43	2.38	0.00	1.69	0.00	1.98	0.00	1.99	0.00	2.26	0.00	2.19	0.00	2.27	0.00	2.31	0.00	0.19	0.00
Sc45	1.63	0.06	1.28	0.09	1.47	0.14	1.47	0.05	1.56	0.01	2.15	0.07	2.08	0.08	3.62	0.30	0.64	0.00
Ti49	0.19	0.012	0.29	0.11	0.26	0.08	0.21	0.01	0.19	0.00	0.28	0.01	0.3	0.01	0.46	0.06	0.1	0.0
V51	4.83	0.69	2.8	0.12	2.84	0.24	2.35	0.07	3.01	0.07	2.67	0.09	3.5	0.2	5.7	0.77	1.65	0.06
Cr53	8.49	0.57	9.3	0.4	8.51	0.64	5.16	0.17	9.22	0.85	5.58	0.22	12.6	0.7	26	7	7.78	0.65
Co59	1.65	0.25	1.25	0.18	1.14	0.14	0.95	0.03	0.83	0.02	0.93	0.06	1.13	0.06	1.1	0.1	2.06	0.08
Ni60	8.5	3.9	26	9	22	8	41	1	13	3	10	3	11	1	10	1	11.3	1.7
Cu65	0.47	0.13	1.4	0.6	1.26	0.00	< 0.5		< 0.5		0.62	0.23	0.9	0.2	1.5	0.2	2.8	0.0
Zn66	0.69	0.17	0.32	0.04	0.31	0.04	0.29	0.01	0.22	0.01	0.27	0.04	0.27	0.02	0.25	0.02	0.66	0.03
Ga71	0.77	0.18	0.45	0.06	0.41	0.04	0.34	0.01	0.24	0.01	0.23	0.02	0.32	0.02	0.34	0.04	0.38	0.02
Ge74	3.27	3.01	1.39	0.15	1.26	0.10	1.13	0.04	1.1	0.03	1.11	0.11	1.7	0.09	1.52	0.04	1.36	0.07
As75	0.31	0.07	0.02	0.01	0.019	0.000	0.024	0.005	0.01	0.00	0.003	0.002	0.15	0.04	0.0075	0.0002	< 0.006	
Rb85	< 0.0002		< 0.0003		0.010	0.001	0.0004	0.0002	0.03	0.004	0.0014	0.0003	0.08	0.01	8E-05	8E-05	0.0038	0.0004
Sr86	0.103	0.003	0.080	0.003	0.095	0.001	0.096	0.003	0.103	0.001	0.100	0.004	0.146	0.006	0.111	0.004	0.0021	0.0003
Sr88	0.104	0.003	0.081	0.003	0.098	0.002	0.098	0.003	0.106	0.000	0.102	0.004	0.147	0.006	0.113	0.003	0.0019	0.0001
Y89	0.340	0.025	0.42	0.09	0.41	0.10	0.42	0.01	0.36	0.01	0.53	0.02	0.39	0.02	0.51	0.05	0.046	0.003
Zr90	0.060	0.003	0.1	0.04	0.089	0.036	0.071	0.002	0.050	0.002	0.110	0.004	0.141	0.005	0.2	0.04	0.0099	0.0005
Nb93	0.0012	0.0000	0.006	0.005	0.006	0.002	0.002	0.000	0.0017	0.0003	0.0035	0.0003	0.057	0.002	0.005	0.001	0.0007	0.0001
Mo98	0.016	0.001	0.016	0.008	0.016	0.005	0.011	0.000	0.009	0.0005	0.0085	0.0006	0.059	0.003	0.012	0.002	0.0039	0.0003
Ag107	0.035	0.053	0.35	0.12	0.33	0.055	0.186	0.011	0.1	0.01	0.029	0.015	0.7	0.2	0.07	0.01	<0.008	
Cd111	0.53	0.529	2.05	0.18	1.45	0.30	1.4	0.07	2.47	0.19	1.25	0.18	1.6	0.4	0.71	0.03	0.48	0.08
In115	3.33	0.00	0.64	0.13	0.52	0.08	0.44	0.01	0.37	0.01	0.44	0.05	0.81	0.04	1.02	0.09	0.24	0.01
Sn118	1.0	0.1	0.18	0.06	0.12	0.05	0.045	0.003	0.030	0.002	0.024	0.003	0.38	0.04	0.037	0.010	0.015	0.003
Sb121	< 6		0.012	0.002	0.017	0.002	0.013	0.001	0.010	0.002	0.004	0.001	0.103	0.008	0.0044	0.0003	0.0011	0.0002
Cs133	0.0002	0.0001	< 0.0001		0.0041	0.001	< 0.0002		0.010	0.003	0.0007	0.0002	0.070	0.006	7E-05	7E-05	0.0009	0.0002
Ba137	0.0003	0.0000	0.00016	4E-05	0.005	0.001	0.0006	0.0001	0.020	0.002	0.0011	0.0001	0.090	0.005	0.00015	8E-05	0.0036	0.0003
La139	0.03	0.001	0.03	0.01	0.039	0.013	0.035	0.001	0.030	0.001	0.047	0.002	0.094	0.004	0.07	0.01	0.0006	0.0001
Ce140	0.057	0.002	0.06	0.02	0.07	0.02	0.064	0.002	0.060	0.002	0.083	0.003	0.126	0.006	0.12	0.02	0.0017	0.0002
Nd146	0.13	0.003	0.15	0.04	0.16	0.04	0.15	0.01	0.140	0.006	0.19	0.01	0.23	0.01	0.27	0.03	0.004	0.0007
Sm147	0.22	0.011	0.25	0.06	0.27	0.05	0.26	0.01	0.24	0.01	0.35	0.01	0.31	0.02	0.42	0.04	0.011	0.000
Tb159	0.33	0.014	0.38	0.09	0.4	0.09	0.40	0.01	0.35	0.01	0.51	0.02	0.45	0.02	0.56	0.05	0.030	0.002
Ho165	0.35	0.02	0.43	0.10	0.45	0.10	0.45	0.01	0.38	0.01	0.56	0.02	0.46	0.02	0.55	0.06	0.048	0.002
Tm169	0.33	0.03	0.43	0.09	0.45	0.10	0.45	0.01	0.35	0.01	0.54	0.02	0.44	0.02	0.48	0.04	0.071	0.003
Yb172	0.25	0.13	0.43	0.1	0.4	0.05	0.39	0.07	0.33	0.05	0.39	0.06	0.52	0.10	0.47	0.03	0.077	0.035
Lu175	0.31	0.04	0.41	0.09	0.42	0.11	0.41	0.01	0.31	0.01	0.49	0.02	0.40	0.02	0.43	0.04	0.090	0.004
Hf177	0.12	0.011	0.2	0.08	0.19	0.08	0.15	0.01	0.11	0.01	0.25	0.01	0.23	0.01	0.42	0.08	0.017	0.002
Ta181	0.0022	0.001	0.02	0.02	0.0145	0.01	0.0052	0.0005	0.0043	0.0005	0.011	0.001	0.07	0.00	0.021	0.008	0.0008	0.0002
W183	0.0005	0.0002	0.0001	0.0001	0.0026	0.0008	0.0010	0.0002	0.0011	0.0002	0.001	0.000	0.05	0.00	0.00027	1E-05	0.0005	0.0001
W184	0.0006	0.0002	0.00015	1E-05	0.0019	0.0002	0.001	0.0001	0.001	0.0001	0.001	0.000	0.05	0.00	0.00014	0.00014	0.0002	0.0001
Tl205	< 1.7		< 0.01		< 0.02		< 0.01		0.017	0.02	< 0.01		0.07	0.03	< 0.01		< 0.01	

Table 3 (Contd.)

	Run 1956		Run R80		Run 1949		Run 1948		Run R78		Run R77		Run 1950		Run R79		1949	
°C	1,180		1,170		1,160		1,160		1,100		1,100		1,050		1,075		1,160	
GPa	3.5		3.0		2.7		2.5		2.5		2.0		2.0		1.0		2.7	
	cpx/melt	1σ	cpx/melt	1σ	cpx/melt	1σ	cpx/melt	1σ	cpx/melt	1σ	cpx/melt	1σ	cpx/melt	1σ	cpx/melt	1σ	opx/melt	1σ
Pb208	< 0.2		0.018	0.002	0.02	0.00	0.014	0.002	0.0136	0.001	0.011	0.002	0.058	0.007	0.008	0.001	< 0.0001	
Bi209	ND		0.055	0.002	0.0854	0.03	0.084	0.004	0.0258	0.005	0.02	0.003	0.42	0.04	0.037	0.018	0.0026	0.0010
Th232	0.0030	0.0003	0.006	0.004	0.0076	0.003	0.0035	0.0005	0.0039	0.0003	0.007	0.001	0.004	0.001	0.007	0.002	0.0005	0.0002
U238	0.0029	0.0001	0.005	0.002	0.0071	0.0015	0.0055	0.0006	0.0041	0.0002	0.007	0.001	0.004	0.001	0.006	0.001	0.0007	0.0003

	1949		R78		1950		1950		1951		1955		1956		R77		R79	
°C	1,160		1,100		1,050		1,050		1,025		1,190		1,190		1,100		1,075	
GPa	2.7		2.5		2.0		2.0		1.0		3.5		3.5		2.0		1.0	
	Mica/melt	1σ	Mica/melt	1σ	Mica/melt	1σ	Amph/melt	1σ	Amph/melt	1σ	garnet/melt	1σ	garnet/melt	1σ	olivine/melt	1σ	olivine/melt	1σ
Li7	0.21	0.01	0.21	0.02	0.19	0.01	0.098	0.005	0.09	0.01	0.041	0.008	0.035	0.01	0.29	0.02	0.42	0.06
Be9	0.07	0.02	0.046	0.010	0.037	0.002	0.14	0.01	0.18	0.01			0.002	0.001	0.001	0.000	0.003	0.001
B10	0.024	0.013	0.015	0.020	0.097	0.009	0.074	0.004	0.05	0.01	0.006	0.002	0.003	0.000	0.02	0.00	0.18	0.03
Mg25	2.19	0.08	2.29	0.05	2.88	0.04	2.02	0.08	2.54	0.14	1.88	0.27	2.32	0.24	0.001	0.000	0.001	0.000
Al27	1.33	0.04	1.35	0.01	1.643	0.004	1.03	0.05	0.89	0.03	1.97	0.16	2.01	0.21	0.002	0.000	0.006	0.003
P31	0.003	0.002	0.0025	0.0016	0.0041	0.0004	0.019	0.002	0.030	0.004	0.034	0.006	0.03	0.004	0.038	0.000	0.05	0.02
Ca43	0.0065	0.0012	0.0041	0.0007	0.01	0.001	1.22	0.00	1.32	0.00	0.87	0.05	0.91	0.014	0.007	0.000	0.02	0.01
Sc45	0.16	0.01	0.16	0.002	0.247	0.002	1.59	0.01	2.86	0.06	4.01	0.57	5.79	0.52	0.22	0.01	0.32	0.02
Ti49	0.79	0.03	0.71	0.02	1.02	0.04	0.72	0.03	1.35	0.05	0.2	0.03	0.15	0.004	0.011	0.000	0.015	0.003
V51	1.55	0.06	1.8	0.08	2.5	0.2	3.4	0.27	5.7	0.5	1.92	0.38	1.93	0.22	0.15	0.02	0.23	0.03
Cr53	3.3	0.3	4.8	0.7	6.2	1.4	7.0	2.7	21	4	8.1	3.2	36	12	0.64	0.05	1.3	0.2
Co59	2.25	0.09	1.91	0.05	3.1	0.1	1.88	0.04	2	0.1	3.7	1.1	3.7	0.5	4.0	0.2	6.6	0.1
Ni60	68.47	10.04	80	17	79	15	32	3	18	2	4.93	3.27	8.78	4.22	32	10	47	5
Cu65	< 0.09		0.5	0.75	2.12	0.06	1.1	0.1	1.8	0.5	0.69	0.05	0.41	0.048	1.19	0.38	4.1	0.1
Zn66	0.52	0.03	0.4	0.03	0.52	0.05	0.33	0.01	0.41	0.03	1.61	0.71	1.63	0.51	0.88	0.12	1.4	0.1
Ga71	0.66	0.03	0.65	0.04	0.81	0.02	0.60	0.04	0.68	0.01	1.02	0.38	1.00	0.23	0.005	0.000	0.012	0.004
Ge74	0.51	0.02	0.54	0.05	1.08	0.05	1.61	0.06	1.19	0.03	ND		ND		0.55	0.000	0.95	0.04
As75	< 0.03		< 0.04		< 0.03		0.044	0.005	0.02	0.01	0.18	0.09	0.13	0.06	0.002	0.000	< 0.009	
Rb85	5.0	0.2	6.2	0.6	7.5	0.4	0.26	0.05	0.1	0.01	< 0.0003		0.002	0.001	< 0.0004		< 0.0004	
Sr86	0.16	0.01	0.140	0.004	0.173	0.003	0.23	0.01	0.42	0.03	< 0.003		0.003	0.001	< 0.0008		0.001	0.001
Sr88	0.16	0.01	0.140	0.004	0.178	0.003	0.24	0.01	0.42	0.03	0.0005	0.0000	0.002	0.001	< 0.00002		0.001	0.001
Y89	0.0030	0.0005	< 0.0003		0.002	0.00	0.38	0.01	0.56	0.02	2.64	0.19	2.8	0.267	0.003	0.000	0.008	0.003
Zr90	0.012	0.001	0.008	0.000	0.011	0.00	0.13	0.01	0.31	0.05	0.14	0.03	0.09	0.008	0.001	0.000	0.002	0.002
Nb93	0.055	0.002	0.047	0.004	0.070	0.002	0.069	0.001	0.21	0.02	0.001	0	0.002	0.000	< 0.00007		< 0.00007	
Mo98	0.046	0.002	0.03	0.00	0.030	0.001	0.0272	0.0003	0.06	0.003	0.003	0.001	0.003	0.000	0.001	0.000	0.0007	0.0001
Ag107	0.043	0.012	0.09	0.01	0.35	0.17	3.01	0.76	1.45	0.6	0.22	0.11	0.07	0.054	0.001	0.000	0.008	0.009
Cd111	0.05	0.02	< 0.02		0.04	0.02	1.12	0.29	0.76	0.09	2.21	1.5	4.74	2.164	0.17	0.03	0.22	0.04
In115	0.14	0.01	0.13	0.01	0.3	0.01	1.09	0.08	2.54	0.21	10.3	9.3	87	50	0.09	0.01	0.20	0.01
Sn118	0.05	0.00	0.034	0.001	0.28	0.01	0.72	0.04	0.11	0.01	0.86	0.16	0.5	0.502	0.002	0.000	0.014	0.004
Sb121	0.0013	0.0002	0.001	0.001	0.005	0.004	0.016	0.001	0.007	0.003	ND		10	14.142	0.0004	0.0003	< 0.0001	
Cs133	2.26	0.14	2.6	0.2	3.2	0.2	0.06	0.02	0.003	0.001	< 0.0001		0.001	0.000	0.0002	0.0002	< 0.0002	
Ba137	3.10	0.13	3.04	0.10	4.1	0.1	0.19	0.03	0.26	0.03	0.0002	0.0001	0.002	0.001	0.0001	0.0001	< 0.0001	
La139	0.0004	0.0001	0.0001	0.0000	0.0004	0.0000	0.05	0.01	0.11	0.01	0.0005	0.0000	0.002	0.000	< 0.0001		< 0.0001	
Ce140	0.0003	0.0001	< 0.00006		< 0.00006		0.09	0.01	0.19	0.01	0.0027	0.0005	0.003	0.001	< 0.0001		0.001	0.001
Nd146	0.0009	0.0004	< 0.0003		0.0002	0.0002	0.20	0.01	0.37	0.02	0.028	0.007	0.02	0.00	< 0.0005		0.003	0.003
Sm147	< 0.0007		< 0.0007		< 0.0007		0.30	0.01	0.54	0.03	0.17	0.04	0.12	0.009	< 0.001		0.002	0.002

Table 3 (Contd.)

	1949		R78		1950		1950		1951		1955		1956		R77		R79	
°C	1,160		1,100		1,050		1,050		1,025		1,190		1,190		1,100		1,075	
GPa	2.7		2.5		2.0		2.0		1.0		3.5		3.5		2.0		1.0	
	Mica/melt	1σ	Mica/melt	1σ	Mica/melt	1σ	Amph/melt	1σ	Amph/melt	1σ	garnet/melt	1σ	garnet/melt	1σ	olivine/melt	1σ	olivine/melt	1σ
Tb159	0.0007	0.0002	0.0003	0.0002	0.0001	0.0001	0.40	0.02	0.64	0.03	1.18	0.17	1.0	0.1	0.0010	1E-05	0.004	0.003
Ho165	0.0009	0.0002	0.0004	0.0002	0.0001	0.0001	0.41	0.02	0.61	0.03	2.66	0.21	2.75	0.3	0.0031	3E-05	0.009	0.004
Tm169	0.0014	0.0002	0.0006	0.0002	0.0005	0.0000	0.36	0.02	0.51	0.02	4.24	0.3	5.26	0.67	0.0091	6E-05	0.018	0.002
Yb172	< 0.035		< 0.035		< 0.035		0.27	0.04	0.44	0.05	5	0.64	6.25	0.75	< 0.05		< 0.05	
Lu175	0.0017	0.0003	0.0016	0.0002	0.0017	0.0002	0.30	0.02	0.44	0.02	5.5	0.79	8.03	1.23	0.024	0.001	0.041	0.003
Hf177	0.015	0.002	0.011	0.000	0.016	0.001	0.27	0.003	0.59	0.15	0.11	0.03	0.06	0.007	0.0008	0.0000	0.004	0.004
Ta181	0.062	0.003	0.047	0.004	0.078	0.004	0.083	0.004	0.24	0.01	0.0017	0.0008	0.0022	0.0005	< 0.0002		0.0004	0.0004
W183	0.0043	0.0004	0.0005	0.0001	0.0006	0.0002	0.0012	0.0001	0.0023	0.0009	0.0008	0.0005	0.0020	0.0006	0.0003	0.0003	< 0.0002	
W184	0.0014	0.0002	0.0004	0.0001	0.0006	0.0001	0.0011	0.0001	0.0025	0.0009	0.0007	0.0004	0.0021	0.0006	0.0003	0.0003	< 0.0001	
Tl205	3.03	0.29	3.45	0.22	5.2	0.3	0.23	0.04	0.11	0.01	ND		ND		< 0.015		0.01	0.01
Pb208	0.089	0.01	0.060	0.005	0.096	0.005	0.07	0.02	0.05	0.01	0.02	0.02	ND		< 0.001		< 0.001	
Bi209	0.016	0.003	0.03	0.01	0.13	0.06	0.14	0.03	0.49	0.6	ND		ND		< 0.002		0.0024	0.0001
Th232	0.0004	0.0002	< 0.0002		< 0.0002		0.0035	0.0008	0.009	0.001	0.0008	0.0000	0.0014	0.0004	0.00017		0.00000 <	0.0003
U238	0.0033	0.0005	< 0.0002		< 0.0002		0.0039	0.0009	0.008	0.001	0.0036	0.0009	0.0035	0.0006	0.00026		0.00017 <	0.0003

1 sigma standard deviations are propagated from 1 sigma errors for replicate analyses of run products. The numerical suffix to each element indicates the particular isotope analysed
ND not determined

probably due it being concentrated in vesicles during preparation of the starting glass. There is no evidence that other (non-volatile) incompatible elements were heterogeneously distributed in the starting material.

Clinopyroxene

The clinopyroxenes from experiments are aluminian-diopsides with variable concentrations of enstatite, tschermaks, jadeite and Ti. Their compositions vary with changes in pressure and temperature (Fig. 1). Clinopyroxenes crystallized at 1.0 GPa are comparatively Ti- and Ca-rich and compositionally similar to green phenocryst cores in the basanite. In contrast, near-liquidus clinopyroxenes formed at 2.5–2.7 GPa are compositionally similar to the clinopyroxenes in garnet lherzolite xenoliths from Bow Hill. They are slightly less aluminous and Cr-rich, and also have lower Mg numbers (Mg no. = 100 Mg/(Mg + total Fe)). They are also noticeably less Cr-rich than the clinopyroxenes crystallized from the same composition by Adam (1989, 1990). This probably reflects some reduction of Cr^{+3} to Cr^{+2} in our experiments.

Partition coefficients for most elements follow patterns similar to those previously obtained for calcic clinopyroxenes and silicate melts (e.g. Hart and Dunn 1993; Liotard et al. 1988; Green et al. 2000; Hill et al. 2000). Ni and Cr are highly compatible and the other siderophile transition elements (including V, Co, Cu and Zn) either mildly compatible or mildly incompatible. Cd tends to partition similarly to Ca whereas Pb more closely follows Sr. Sc, In and Ga also vary from mild compatibility to incompatibility. Y and heavy rare earth elements (HREE) are moderately incompatible, with compatibility varying as a smooth function of ionic radius. The light rare earths, Th and U are far more incompatible. Bi behaves similarly to the LREE whereas Sb and Mo behave similarly to Nb and Ta. Considering that cassiterite and rutile are isostructural the compatibility of Sn in some experiments

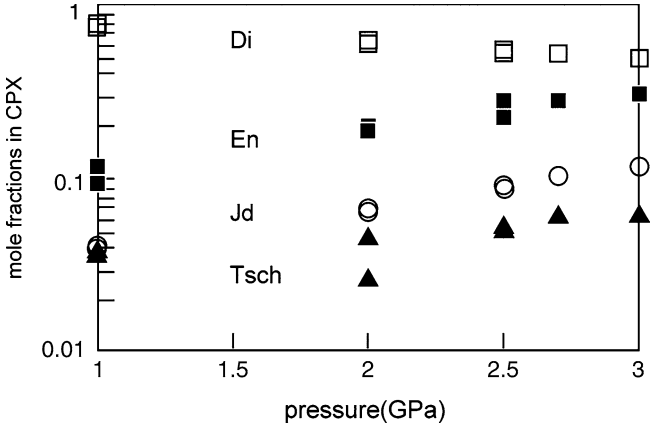

Fig. 1 Variation in clinopyroxene compositions with changes in pressure

was surprisingly small when compared to Ti. Partition coefficients for W, Rb, Cs and Ba, although sensitive to analytical contamination, appear to be very small (generally < 0.001). The partition coefficients of most elements also vary with changes in pressure, temperature and mineral composition. These changes are described more fully in a later section.

Orthopyroxene

Orthopyroxenes from the Bow Hill basanite contain minor concentrations (0.17–0.31 wt%) of TiO_2 and Na_2O, and are less aluminous than coexisting clinopyroxenes. Like clinopyroxenes they tend to become more aluminous with increasing pressure and temperature. With the exception of Mg and the siderophile elements Cr, Ni, Co, Cu and Zn, partition coefficients for most elements are smaller than for clinopyroxenes. Partition coefficients for the REE in particular are much smaller with the peak in partition coefficient values being shifted toward the heavier REE.

Olivine

Some of the olivines analysed during this study have relatively low Mg numbers when compared to coexisting clinopyroxenes. This appears to reflect a degree of unsampled heterogeneity since satisfactory mass balances with the starting compositions could only be obtained when forsterite was added to the list of run products. All of the olivines contain small concentrations of TiO_2, Al_2O_3 and Cr_2O_3 that can be detected with both the electron microprobe and LAM ICP-MS. They also contain minor concentrations of NiO, MnO and CaO. Partition coefficients for elements other than Ni, Mg, Fe, Co, Mn, Co, Cu and Zn are mostly small. A notable exception is Li. Nevertheless meaningful partition coefficients were determined for a broad range of other elements including Be, B, P, Ge, Ca, Cd, In, Sc, Y and HREE.

Amphibole

The experimentally produced amphiboles are chiefly of mixed pargasite and kaersutite composition. Amphibole was the most accommodating mineral studied in terms of its ability to incorporate a broad range of minor and trace elements, including F, Cl, HFSE, REE, Tl, and the large ion lithophile elements (LILE) K, Rb, Cs and Ba.

Mica

The micas from experiments are all tri-octahedral phlogopites with only limited substitutions of di-octahedral components. They show relatively little compositional variation. Like amphibole they partition Nb and Ta more strongly than coexisting clinopyroxenes. They also strongly incorporate Cs, Rb, K, Ba, Ni and Cr. In contrast, partition coefficients for Ca, Sr, Cd and REE are very small. Concentrations of F and Cl in mica are up to twice those of coexisting amphibole.

Garnet

Garnets are dominantly of mixed pyrope, almandine and grossular composition (*alm* 19.3–23.1, *py* 63.4–60.6 and *gr* 17.3–16.3) with minor TiO_2, MnO and Na_2O. They are slightly more calcic and Ti-rich than the garnets in garnet lherzolite xenoliths from Bow Hill and other alkaline basalt occurrences (see Sutherland et al. 1984; Xu et al. 1998) otherwise they differ mainly in their relatively low Mg numbers (76.6–72.4). The crystals from individual experiments are relatively homogeneous in all elements including the HREE. As found in many previous studies of garnet (e.g. Irving and Frey 1984; Hauri et al. 1994; van Westrenen 1999) their partition coefficients are characterized by a combination of very small values for LILE and steeply inclined REE patterns that increase with atomic number.

Discussion

The effects of pressure, temperature and crystal chemistry on partition coefficients

The effects of pressure and temperature on mineral compositions and partition coefficients are most evident for clinopyroxene since this mineral crystallized over the widest range of conditions. One of the most notable features of the data for clinopyroxene is the amount of covariation between variables. There are near-linear correlations between the log-normalized concentrations of enstatite, diopside, jadeite, tschermaks and pressure for pressures of 1.0–3.0 GPa (Fig. 1). Because of the tendency for temperature to increase with pressure in our experiments, there are similar although less consistent correlations with temperature. For the alumina-enriched composition at 3.5 GPa, the clinopyroxenes are slightly more calcic but less aluminous than indicated by the previously described trends. Ti concentrations are highest for the clinopyroxenes produced at 1.0 GPa and 1,025–1,075°C but otherwise any relationship to pressure and temperature is not obvious. The more limited data for olivine, orthopyroxene, amphibole and mica also show some evidence of the effects of pressure and temperature on composition. Olivine becomes less calcic and orthopyroxene more aluminous as pressure increases; amphiboles also become richer in SiO_2 and alkalis, but poorer in Al^{iv}, TiO_2, Cr_2O_3 and CaO. TiO_2 concentrations in micas decrease slightly as pressure and temperature both increase.

The changes in mineral composition are accompanied by changes in the partition coefficients of most elements.

However, when considered element by element these changes are less systematic than the changes in major elements; this is due to their multidependence which makes it difficult to correlate partition coefficients with single variables. The systematic nature of the interrelationships between partition coefficients, pressure, temperature and mineral chemistry are only fully apparent when the different factors influencing partition coefficients are isolated and considered separately. To do this, we separately examine the effects of:

1. Cation radius and lattice-strain
2. Cation valence and coulombic potentials

When examining these factors, we also note their relationship to mineral composition and the way that this is also related to pressure, temperature and H_2O concentrations. The effect of H_2O concentration on melting relationships is also considered.

Cation radius and lattice-strain

The systematic influence of cation radius, combined with the radius and elastic properties of cation sites, on partition coefficients has been described by many authors (e.g. Onuma et al. 1968; Brice 1975; Blundy and Wood 1994). These relationships were quantified by Blundy and Wood (1994) who used the general relationship

$$D_i = D_0 \exp((-4\pi E N_A [r_0/2(r_i - r_0)^2 + 1/3(r_i - r_0)^3])/(RT)) \quad (1)$$

to describe the Nernst partition coefficients (D_i) for isovalent cations in crystals and melts as a function of cation radius (r_i), the radius of the crystallographic site occupied by the cations (r_0), the partition coefficient (D_0) of the ideal or fictive cation having radius r_0, and an elastic constant E (Young's modulus) that is specific to the host cation site. N_A, R and T stand for Avogadro's constant, the universal gas constant, and temperature (K), respectively.

In order to apply the lattice-strain model to our own data a number of simplifying assumptions and strategies were necessary. Ideally the lattice-strain model is applicable to crystals whose cations and anions are held together by ionic bonds. It does not account for other types of bonding, localization of electrical charge, the effects of lattice distortion or the influence of the melt phase. Thus, use of the model implies acceptance of both a degree of approximation and of exceptions to a predicted pattern of behaviour. On Onuma diagrams (plots of D_i versus cation radius) the partition coefficients of most elements follow smooth parabolic trends, consistent with the predictions of the lattice-strain model. But Ni^{+2} and Cr^{+3} plot well above neighbouring isovalent cations, whereas Ga^{+3}, Sn^{+4}, Cd^{+2} and Cu^{+2} show converse behaviour. Some elements, including Sn, Pb, Bi, Cd and Tl are also inconsistent in their behaviour. In each of these cases, we assumed that there were specific factors, unaccounted for by the lattice-strain model, that affected the measured partition coefficients. Thus, these listed elements were not used to find fits for the lattice-strain model.

Because Mo, W, Sb and V can all exist in a variety of valence states, deciding on their probable valence states during experiments was a problem. In most cases, the partitioning of Mo and Sb follow the partitioning of Nb and Ta. As the latter are usually assumed to be pentavalent and have similar pentavalent radii to Mo and Sb, we assumed that Mo and Sb were also pentavalent. In scheelite and wolframite W is hexavalent. As this seemed to accord with the very low partition coefficients that we obtained for W in our experiments we also assumed that W was hexavalent. Relative to pyroxenes, amphiboles and micas partition coefficients for V in olivine are not large (0.15–0.23). Therefore, most of the V in experiments seems likely to have been present as V^{+3} rather than V^{+2}. This option also gives the smoothest and most consistent results when V is plotted on Onuma diagrams.

The Young's Modulus E could in most cases be determined from fits to Eq. 1. However, for some isovalent series its value was either difficult to determine due to lack of sufficient data, or unexpected. Generally it has been found in past studies (e.g. Blundy and Wood 2003) that E increases with cation valence and this is consistent with what we found in this study. But for + 5 ions in sites of octahedral coordination, E is either very much higher than would be predicted from the trends for lower valenced cations, or the tightness of the Onuma diagrams for + 5 cations is a function of factors in addition to E. This makes precise determinations of r_0 for + 5 cations difficult, although it has relatively little effect on the determinations of D_0^{+5}.

No attempt was made to either take account of or model split site behaviour. Instead a different approach was taken and all octahedral and ten to 12-fold sites in amphiboles and micas were treated as single sixfold and tenfold sites. This was done for practical reasons as we were unable to discriminate individual site occupancies in these cases. We also wanted to be able to use the derived D_0^{+n} values to model the effects of cation valence and coulombic potentials.

We successfully fitted the lattice-strain model to partition coefficients for all of the minerals produced in this study. However, because most of our results are for clinopyroxene, the following discussion is mostly about the results for this mineral. Values of D_0, r_0 and E found by fitting Eq. 1 to the data in Table 3 are shown in Table 4. Examples of fitted solutions for clinopyroxene and amphibole are shown graphically in Figs. 2a and 3a alongside the plotted values of measured partition coefficients. Partition coefficients for the large majority of elements (data for Ni, Cr, Sn and Ga excepted) are approximated to within ± 20% by our fits to the lattice-strain model, with over half within ± 10%. The graphical representations show how strongly the partition coefficients of different minerals are controlled by the properties of individual crystallographic sites. These

Table 4 D_0^{+n}, r_0^{+n}, E^{+n}, ΔG^{coulb}, optimum valence and, $D_0^{\Delta e=0}$ calculated from partition coefficient data

Run °C	1956		R80		1949		1948		R78		R77		1950		R79		1949	
GPa	1,180		1,170		1,160		1,160		1,100		1,100		1,050		1,075		1,160	
	3.5		3.0		2.7		2.5		2.5		2.0		2.0		1.0		2.7	
	cpx		cpx		cpx		cpx		cpx		cpx		cpx		cpx		opx	
	M1	M2	M1	M2	M1	M2	M1	M2	M1	M2	M1	M2	M1	M2	M1	M2	M1	M2
D_0^{+6}	0.00015		0.0027		0.0011		0.0012		0.001		0.05		0.00027		0.0004			
r_0^{+6}	0.59		0.595		0.59		0.59		0.595		0.59		0.6		0.59			
E^{+6}	7,000		4,800		5,000		5,000		7,000		7,000		6,400		4,800			
D_0^{+5}	0.003		0.02		0.018		0.013		0.01		0.011		0.066		0.025		0.005	
r_0^{+5}	0.61		0.62		0.607		0.605		0.6		0.62		0.62		0.63		0.59	
E^{+5}	3,500		4,000		5,000		5,000		7,000		5,000		3,500		3,500		6,000	
D_0^{+4}	0.4	0.0035	0.65	0.007	0.6	0.0084	0.47	0.0057	0.37	0.0046	0.67	0.008	0.7	0.005	1.1	0.008	0.14	0.0007
r_0^{+4}	0.652	1.02	0.652	1.018	0.65	1.029	0.652	1	0.65	1.023	0.655	1.025	0.655	1.02	0.655	1.031	0.63	0.89
E^{+4}	1,600	600	1,600	800	1,600	600	1,600	600	1,600	600	1,600	800	1,600	800	1,600	800	1,500	600
D_0^{+3}	5.2	0.36	3.8	0.48	3.7	0.46	3.3	0.45	3.7	0.38	3.8	0.57	4.5	0.47	7.3	0.58	2.2	0.14
r_0^{+3}	0.665	1.012	0.67	1.006	0.677	1.01	0.68	1.01	0.675	1.019	0.685	1.01	0.684	1.028	0.697	1.03	0.68	0.8
E^{+3}	700	290	600	300	560	290	610	300	580	330	690	290	710	270	800	330	600	340
D_0^{+2}	3	2.6	2.8	2.1	1.8	2.4	1.5	2.5	1.9	2.8	2.4	2.55	2.5	2.5	2.2	3.1	2.8	0.9
r_0^{+2}	0.67	1.063	0.665	1.063	0.665	1.066	0.69	1.067	0.665	1.072	0.665	1.067	0.665	1.077	0.665	1.069	0.67	0.86
E^{+2}	400	220	400	220	350	220	400	240	410	260	400	230	400	220	400	280	450	160
D_0^{+1}		0.55		0.5		0.64		0.4		0.47		0.45		0.27		0.21		0.29
r_0^{+1}		1.05		1.165		1.11		1.1		1.08		1.06		1.07		1.07		0.88
E^{+1}		120		80		70		1.1		95		140		55		55		120
ΔG^{coulb}	12.86	18.49	12.09	16.33	12.97	16.21	12.44	18.44	12	17.86	13.09	18.23	8.57	18.65	13.72	19.17	9.92	19.17
Optimum valence	2.68	2.40	2.67	1.97	2.78	1.96	2.72	2.03	2.64	1.99	2.68	2.02	2.68	2.1	2.87	2.16	2.2	1.88
$D_0^{\Delta e=0}$	5.00	2.00	4.28	1.95	3.53	2.26	2.83	2.18	3.13	2.25	4.16	2.28	3.63	2.14	6.00	2.29	3.2	1.00

Run °C	1950		1951		1949		R78		1950		R79		R77		1955		1956	
GPa	1,050		1,025		1,160		1,100		1,050		1,075		1,100		1,190		1,180	
	2.0		1.0		2.7		2.5		2.0		1.0		2.0		3.5		3.5	
	amph		amph		Mica		Mica		Mica		Olivine		Olivine		Garnet		Garnet	
	M1–3	M4	M1–3	M4	M	A	M	A	M	A	T	M1–2	T	M1–2	Y	X	Y	
D_0^{+6}	0.0011		0.002		0.0015		0.0004		0.0006						0.0007		0.0007	
r_0^{+6}	0.59		0.59		0.6		0.6		0.6						0.595		0.595	
E^{+6}	8,000		8,000		6,000		6,000		6,000						7,000		7,000	
D_0^{+5}	0.083		0.24		0.07		0.05		0.09						0.003		0.003	
r_0^{+5}	0.625		0.63		0.62		0.63		0.63						0.605		0.605	
E^{+5}	8,000		8,000		9,000		9,000		9,000						4,000		4,000	
D_0^{+4}	1.5	0.004	2.5	0.009	1.4		1.2		2		16	0.015	0.008	0.67	1.1	0.004	1.1	0.004
r_0^{+4}	0.645	1.02	0.645	1.03	0.63		0.63		0.63		0.33	0.605	1.025	0.655	0.66	0.99	0.66	0.99
E^{+4}	1,600	800	1,600	800	3,000		3,000		3,500		6,000	1,600	800	1,600	2,400	1,200	2,400	1,200
D_0^{+3}	7	0.41	8	0.64	2.1		2.6		4		0.02	0.3	0.57	3.8	3.8	5.6	3.8	5.6
r_0^{+3}	0.69	1.03	0.7	1.035	0.67		0.675		0.68		0.34	0.74	1.01	0.685	0.59	0.955	0.59	0.955
E^{+3}	750	320	750	300	700		800		850		4,000	470	290	690	1,200	600	1,200	600
D_0^{+2}	3.5	1.4	4	1.4	2.7	3.2	2.5	3.1	4.4	4		6.6		2.4	2.8	4	2.8	4
r_0^{+2}	0.66	1.08	0.66	1.07	0.675	1.62	0.68	1.62	0.67	1.61		0.77		0.665	0.67	1	0.67	1
E^{+2}	400	160	400	160	380	160	400	170	530	170		400		400	800	330	800	330
D_0^{+1}		0.28		0.18	0.25	5.4	0.25	6.1	0.22	7		0.43				0.065		0.065
r_0^{+1}		1.1		1.08	0.7	1.725	0.7	1.73	0.7	1.73		0.78				1.02		1.02
E^{+1}		90		80	200	58	200	55	200	58		250				160		160
ΔG^{coulb}	9.16	16.79	9.16	16.79	10.43		10.46		10.08			19.89		20.26				
Optimum valence	2.75	2.05	2.89	2.18	2.8		2.8		2.82			2.15		2.15				
$D_0^{\Delta e=0}$	7.00	1.50	8.00	1.60	4.40		4.40		6.00			2.50		2.50				

Values for ΔG^{coulb} are in kJ

properties vary both from mineral to mineral and with changes in pressure and temperature.

Except the results for run 1956, r_0^{+3} and r_0^{+4} for clinopyroxene M1 sites correlate negatively with pressure but positively with the average ionic radius of cations in the same site (Fig. 4a, b). The variation in r_0^{+3} is far more evident than for r_0^{+4}. In the case of run 1956, the value of r_0^{+3} is poorly constrained and probably inaccurate. r_0 values for +2 and +5 cations are also insufficiently well determined to show any meaningful correlation. In the case of M2 sites (Fig. 4c, d) r_0 also decreases with increasing pressure, but the

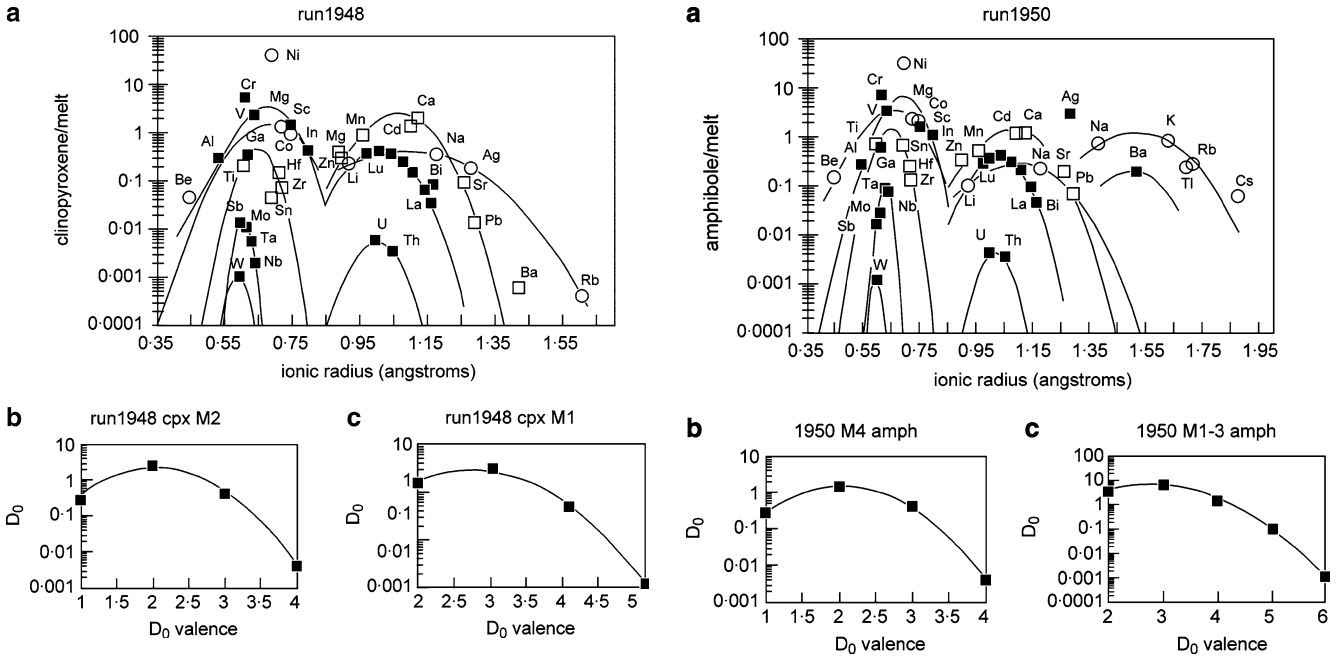

Fig. 2 Measured partition coefficients and fitted solutions to the lattice-strain model (**a**) and D_0^{+n} versus cation valence for M1 and M2 sites (**b**, **c**) in clinopyroxene from run 1948

Fig. 3 Measured partition coefficients and fitted solutions to the lattice-strain model (**a**) and D_0^{+n} versus cation valence for M4 and M1–3 sites (**b**, **c**) in amphibole from run 1950

relationship between r_0 and average ionic radius is not as direct as it is for M1 sites. At low values, r_0^{+2} is larger than the average ionic radius, but gradually approaches the latter up to an average ionic radius of about 1.07–1.08 Å. Above this value r_0^{+2} remains relatively constant in spite of further increases in average cation radius. A similar effect was described by Cameron and Papike (1980) who investigated variations in mean M1–O distances determined from X-ray diffraction measurements. They concluded that site radii are influenced by interactions between the oxygen anions of the pyroxene lattice as well as by cation radii. Thus for cation radii less than about 1.07–1.08 Å

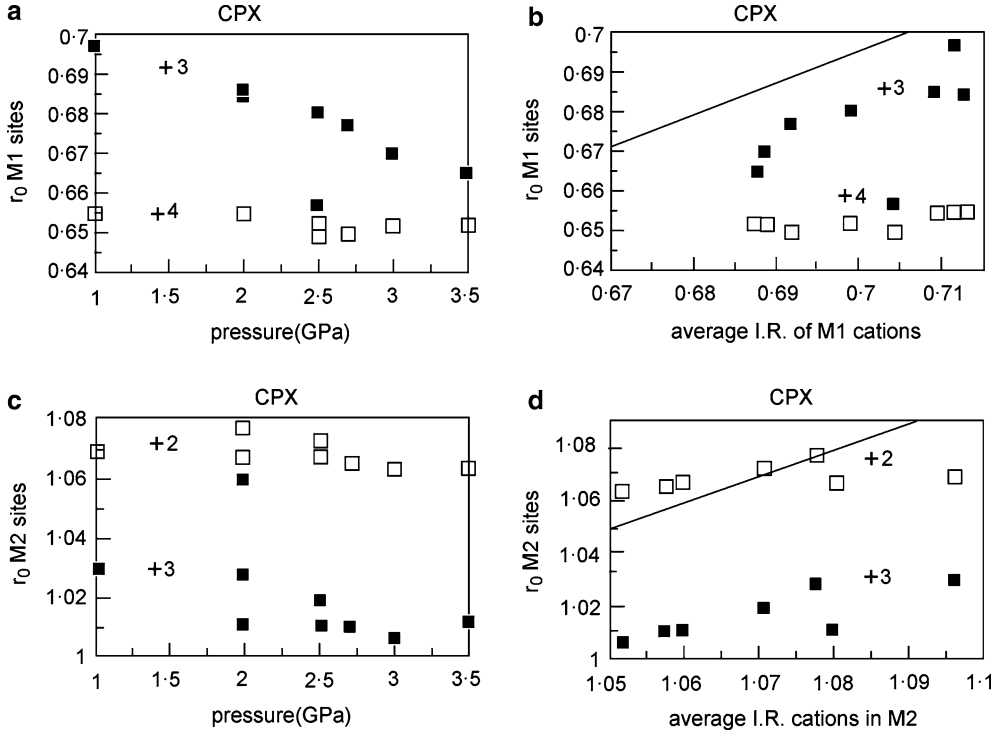

Fig. 4 **a**–**d** r_0^{+n} versus pressure and average ionic radius (weighted according to site occupancy) for clinopyroxene M1 and M2 sites. *Straight lines* for (**b**) and (**d**) mark 1:1 correlations between r_0 and average ionic radii

cations in M2 sites do not completely fill the site. Above this value further increases in the radius of the site are limited by the rigidity of the oxygen lattice so that cations are effectively squeezed.

Cation valence and coulombic potentials

When D_0^{+n} values are plotted against valence they follow a parabolic trend (Figs. 2b, c, 3b, c). Wood and Blundy (2001) also observed this trend for clinopyroxene M2 sites and described it using the relationship

$$D_0^{+n} = D_0^{\Delta e=0}\exp((-\Delta G^{\text{coulb}}\Delta e^2)/RT), \quad (2)$$

where Δe = cation valence minus optimum site valence; ΔG^{coulb} is the coulombic potential energy (J/Δe^2/mol) produced by substituting a cation of mismatched valence; $D_0^{\Delta e=0}$ is the value of D_0 when $\Delta e = 0$; R is the universal gas constant; and T is temperature (K).

The exception to these relationships for the Bow Hill data set is garnet. In this case, the relationships are only approximated, so it is not possible to derive precise values of $D_0^{Delat\ e=0}$ and ΔG^{coulb} (Table 4) by fitting Eq. 2 to D_0^{+n} values. As ΔG^{coulb} becomes larger the parabola described by Eq. 2 becomes tighter. Its value varies depending upon the crystallographic site and mineral, and also with changes in mineral composition. For example, ΔG^{coulb} is consistently larger for eightfold than sixfold sites in clinopyroxenes and amphiboles. In the case of clinopyroxene M2 sites, it also correlates negatively with bulk mineral Al_2O_3 (Fig. 5b). For M1 sites (Fig. 5a) the variation is less evident and any correlation between ΔG^{coulb} and Al_2O_3 appears to be positive rather than negative.

The cause of variations in ΔG^{coulb} is a subject that was addressed by Wood and Blundy (2001). They proposed that ΔG^{coulb} is related to the concentrations of charge-balancing cations in adjacent (next-nearest neighbour) cation sites. This means that for each site population (e.g. the population of M2 sites in a particular clinopyroxene) there will be a range of optimum valences. Each individual site will have only a single value but this will vary from site to site producing a distribution of values. As the valences of charge-balancing cations in adjacent sites become more variable, the scatter of optimum valences for the central cation population becomes greater. This causes a reduction in the average value of Δe^2 and thus also in the overall coulombic potential energy for the site. This general principle is consistent with the positive linear relationship observed between ΔG^{coulb} for M2 sites in clinopyroxene and Al_2O_3 concentrations. But the same relationship is not apparent for clinopyroxene M1 sites. It is also necessary to explain the large differences in ΔG^{coulb} for clinopyroxene M2 and M1 sites and for amphibole M4 and M1–3 sites. Presumably these contradictory relationships reflect aspects of the way cations are distributed and ordered within pyroxenes and amphiboles.

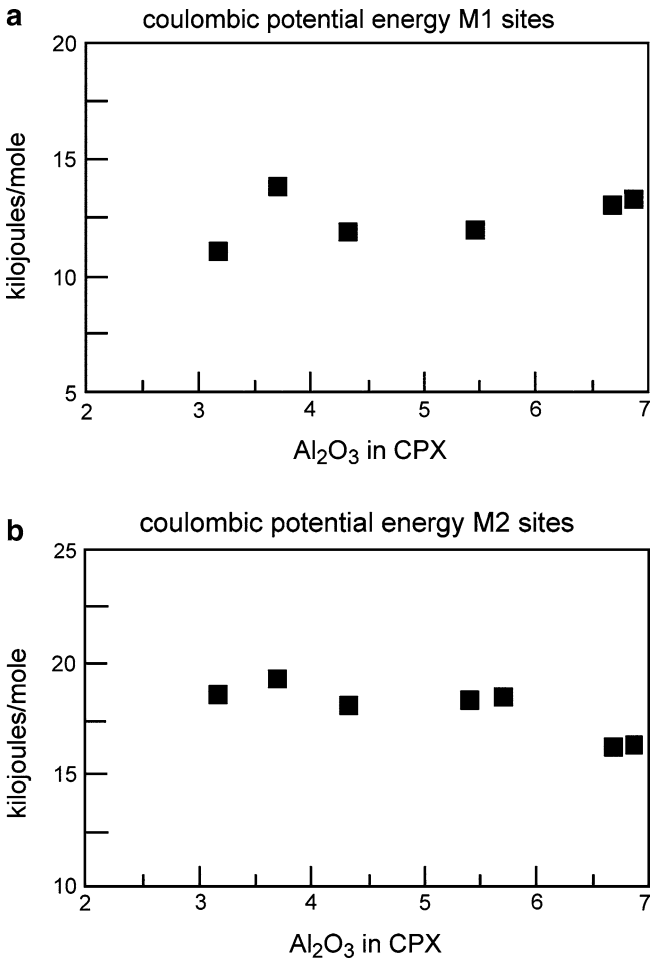

Fig. 5 a, **b** Coulombic potential energy (J/Δe^2/mol) for clinopyroxene M1 and M2 sites

The problem of cation distribution in next-nearest neighbour sites can be indirectly approached by inverting the procedure used by Wood and Blundy (2001). This involves using D_0^{+n} values to calculate optimum valence distributions for individual M2 and M1 site populations. In order to do this Eq. 2 must be expanded to take into account multiple values of Δe^2. This is described by the relationship

$$D_0^{+n} = \exp[-(\Delta G_0 + X^{\Delta e=1}\Delta G^{\text{coulb}} + 4X^{\Delta e=2}\Delta G^{\text{coulb}} + 9X^{\Delta e=3}\Delta G^{\text{coulb}} + \text{etc})/RT], \quad (3)$$

where ΔG_0 is the Gibbs free energy of the partitioning reaction for a hypothetical cation that has both optimum radius and optimum valence. $X^{\Delta e=n}$ is the fraction of sites for which $\Delta e = n$, and $n = \pm 1, \pm 2, \pm 3$ etc. ΔG^{coulb} differs from the same values derived using Eq. 2 by representing a real rather than an apparent value.

Before applying Eq. 3 to our data, we independently estimated the (real) value of ΔG^{coulb} for clinopyroxene M2 sites. We did this by interpolating the linear relationship between ΔG^{coulb} for M2 sites and Al_2O_3 to zero Al_2O_3. The resulting clinopyroxene composition is very

close to pure diopside-hedenbergite. Thus, the effects of variations in local charge balance on ΔG^{coulb} should be minimal. With this value (~23,200 J/Δe^2/mol) it was possible to iteratively search for appropriate values of ΔG_0 and $X^{\Delta e=n}$. For M1 sites we derived a separate value of ΔG^{coulb} by multiplying the value for M2 sites by the ratio of average M1–O and M2–O distances (using r_0 + 1.38). This was based on the linear relationship between coulombic potential energy and distance. The M1 value derived in this way (26,500 J/Δe^2/mol) is only slightly larger than the value for M2 sites. Using the approach just outlined, we found that a normal (or Gaussian) distribution of optimum valences most closely fits the observed variations in D_0^{+n} for each site. Thus, the observed or apparent variations in ΔG^{coulb} for different sites can be related to the 1 sigma standard deviations of optimum valences for individual site populations.

The normal distribution of optimum valences for individual sites is consistent with simple probability effects playing a significant role in determining patterns of cation ordering, as suggested by Wood and Blundy (2001). However, the differences in ΔG^{coulb} for clinopyroxene M1 and M2 sites indicate that these effects do not operate equally throughout the crystal structure. This may be because longer range patterns of ordering exert a controlling influence on local patterns of cation ordering. In the case of clinopyroxene M1 sites, this may render the effects of variations in Al_2O_3 and other components self-compensating. Different but similarly non-random patterns of ordering may also characterize garnets and explain their apparent deviation from the relationships expressed by Eq. 2 (see van Westrenen et al. 2003a, b).

There is another factor affecting cation distributions that is worth mentioning. This is the specificity of some charge-balancing relationships. An example is the close linear correlation between Al^{vi} and Na. In contrast, other +3 cations in M1 sites, such as Ga^{+3}, Sc^{+3} and In^{+3}, do not correlate well with Na but instead correlate with Al^{iv}.

Like ΔG^{coulb} optimum valence also varies for different sites and with changes in mineral composition. It is always larger for clinopyroxene M1 than M2 sites. For M1 sites it correlates linearly with Al^{iv} (Fig. 6b) but for M2 sites the relationship to composition is more complex. In the latter case, optimum valence seems to be a function of both Al^{iv} and Al^{vi} and there is an approximately linear correlation between optimum valence and Al^{iv}/Al^{vi} (Fig. 6c). The combined influence of Al^{iv} and Al^{vi} may underly a similar covariation between optimum valence for M2 sites and Ti–0.1Na (Fig. 6d).

The various influences on $D_0^{\Delta e=0}$ are difficult to clearly identify within the spread of the experimental data. To some extent $D_0^{\Delta e=0}$ is a function of ΔG^{coulb} since if all other things are equal the height of the parabola described by function (2) is inversely proportional to its width. $D_0^{\Delta e=0}$ is also affected by the activities of mineral-forming components in the melt phase and these are influenced by pressure, temperature and H_2O concentration. However for actual liquidus conditions the effects of pressure, temperature and H_2O concentration are largely self compensating since the ΔG of melting of the bulk composition is always equal to zero. For conditions close to the basanite liquidus (82–91% melting) both $D_0^{\Delta e=0}$ and ΔG^{coulb} for clinopyroxene M1 sites decrease as pressure and temperature increase.

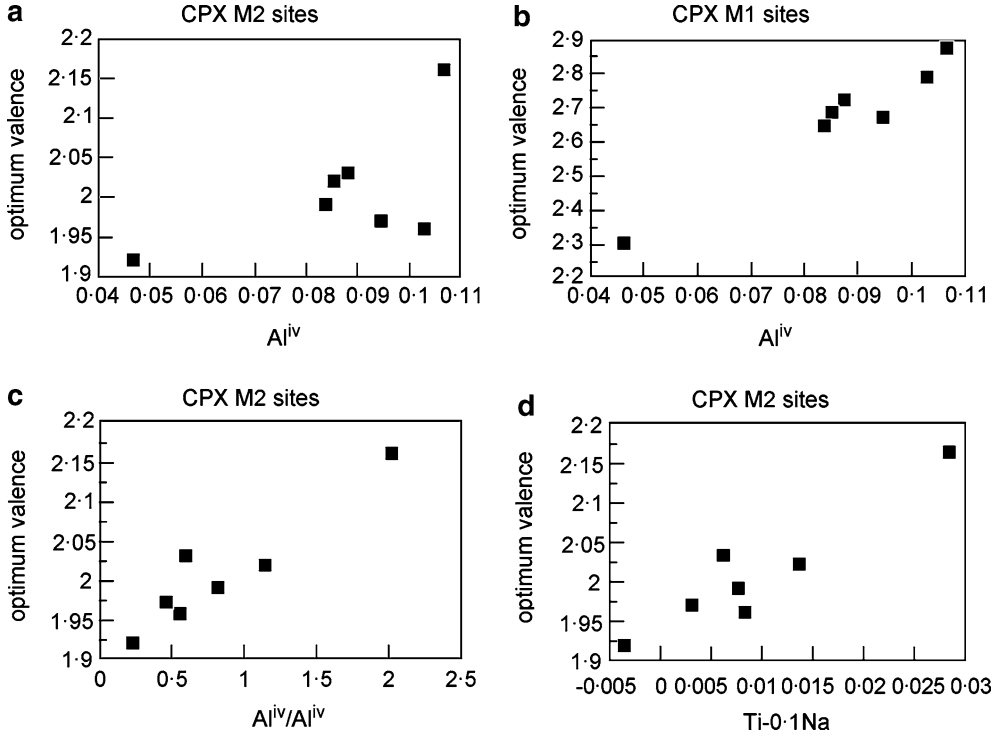

Fig. 6 a–d Optimum valence versus pyroxene composition for clinopyroxene M1 and M2 sites

Generally $D_0^{\Delta e=0}$ increases with increasing degree of crystallization, although run 1950 (which contains coexisting orthopyroxene and amphibole) is an exception to this. $D_0^{\Delta e=0}$ for clinopyroxene M2 sites is much less variable than for M1 sites and generally correlates with D_{Ca}.

The relative effects of H_2O and temperature on $D_0^{\Delta e=0}$ at constant pressure and degree of crystallization can be compared for two runs (1948 and R78). There are only small differences in $D_0^{\Delta e=0}$ for clinopyroxenes from the two runs (see Table 4). This is broadly consistent with Wood and Blundy's (2002) finding that, for constant degrees of crystallization, the effects of increasing temperature and H_2O on partition coefficients are comparable.

Conclusions

Partition coefficients for more than 35 major, minor and trace elements in experimentally produced micas, amphiboles, garnets, clinopyroxenes, orthopyroxenes, olivines and hydrous basanitic melts can be systematically related to cation radius, valence, mineral composition, pressure and temperature. This is most convincingly demonstrated for clinopyroxene. Log-normalized concentrations of enstatite, jadeite and tschermaks in clinopyroxene increase as approximately linear functions of pressure, whereas diopside concentrations decrease in the same manner. Less consistent correlations also occur with temperature. Olivines become less calcic and orthopyroxenes more aluminous as pressure increases; amphiboles also become richer in SiO_2 and alkalis, but poorer in Al^{iv}, TiO_2, Cr_2O_3 and CaO.

The changes in mineral composition are accompanied by changes in a number of crystal-chemical parameters that affect partition coefficients. These include r_0, optimum valence and ΔG^{coulb}. The optimum ionic radius, r_0, for clinopyroxene M1 and M2 sites decreases with increasing pressure. It also correlates positively with the average ionic radius of cations in M1 and M2 sites. ΔG^{coulb}, the coulombic potential energy produced by substituting a cation of mismatched valence into a crystallographic site, is always larger for M2 than M1 sites; in the case of M2 sites, it correlates negatively with Al_2O_3. These variations can be quantitatively modelled as a function of the 1 sigma standard deviations of optimum valences for individual M1 and M2 site populations. The (average) optimum valence of clinopyroxene M1 sites is a positive function of Al^{iv}, whereas for M2 sites it varies as a function of both Al^{iv} and Al^{vi}. ΔG^{coulb} for clinopyroxene M2 sites correlates positively with Al_2O_3 but for M1 sites is less variable.

The systematic interrelationships between partition coefficients and other factors observed in this study, demonstrates both the quality and consistency of our data set. The consistency of the interrelationships also makes it possible to predict the effects of any deviations from the inferred conditions of garnet lherzolite saturation at approximately 1,200°C and 2.6 GPa. It is thus possible to compile a comprehensive set of partition coefficients that will be directly relevant to the formation of the Bow Hill basanite magma by partial melting of garnet lherzolite. These will enable effective constraints to be placed on possible mantle source compositions for the Bow Hill basanite, and on the nature of melting processes during formation of the basanite magma.

Acknowledgements The research for this study was undertaken with the help of on ARC Small Grant and a Macquarie University Research Grant to Trevor Green. We thank Dr Norm Pearson, Suzie Elhou and Carol Lawson for their assistance with electron microprobe and LAM ICP-Ms analyses. Both Jon Blundy and Greg Yaxley are thanked for their reviews of this paper. The graphite capsules and associated furnace components used in this study were manufactured by Rob Roy in the engineering workshop at Macquarie University. This is publication number 429 in the Australian Research Council National Key Centre for the Geochemical Evolution and Metallogeny of Continents (GEMOC).

References

Adam J (1989) Experimental studies of alkaline basalt genesis (unpublished Ph.D. thesis). University of Tasmania, Tasmania

Adam J (1990) The geochemistry and experimental petrology of sodic alkaline basalts from Oatlands, Tasmania. J Petrol 31:1201–1223

Adam J, Green TH (1994) The effects of pressure and temperature on the partitioning of Ti, Sr and REE between amphibole, clinopyroxene and basanitic melts. Chem Geol 117:219–233

Adam J, Green TH, Sie SH (1993) Proton microprobe determined partitioning of Rb, Sr, Ba, Y, Zr, Nb and Ta between experimentally produced amphiboles and silicate melts with variable F content. Chem Geol 109:29–49

Blundy JD, Wood BJ (1991) Crystal-chemical controls on the partitioning of Sr and Ba between plagioclase feldspar, silicate melts and hydrothermal solutions. Geochim Cosmochim Acta 55:193–209

Blundy JD, Wood BJ (1994) Prediction of crystal-melt partition coefficients from elastic moduli. Nature 372:452–454

Blundy JD, Wood BJ (2003) Partitioning of trace elements between crystals and melts. Earth Planet Sci Lett 210:383–397

Boyd FR, England JL (1960) Apparatus for phase-equilibrium measurements at pressures up to 50 kb and temperatures up to 1750°C. J Geophys Res 65:741–748

Brey GP, Green DH (1975) The role of CO_2 in the genesis of olivine melilitite. Contrib Mineral Petrol 49:93–103

Brice JC (1975) Some thermodynamic aspects of strained crystals. J Cryst Growth 28:249–253

Cameron M, Papike J (1980) Crystal chemistry of silicate pyroxenes. In: Prewitt CT (ed) Pyroxenes, Rev Mineral 7:5–92

Gaetani GA, Grove TL (1995) Partitioning of rare earth elements between clinopyroxene and silicate melt: crystal-chemical controls. Geochim Cosmochim Acta 59:1951–1962

Green DH (1973) Conditions of melting of basanite magma from garnet peridotite. Earth Planet Sci Lett 3:247–254

Green TH, Pearson NJ (1985) Rare earth element partitioning between clinopyroxene and silicate liquid at moderate to high pressure. Contrib Mineral Petrol 91:24–36

Green TH, Ringwood AE, Major A (1966) Friction effects and pressure calibration in a piston-cylinder apparatus at high pressure and temperature. J Geophys Res 71:3589–3594

Green TH, Blundy JD, Adam J, Yaxley GM (2000) SIMS determination of trace element partition coefficients between garnet, clinopyroxene and hydrous basaltic liquids at 2–7.5 GPa and 1080–1200°C. Lithos 53:165–187

Hart SR, Dunn T (1993) Experimental cpx/melt partitioning of 24 trace elements. Contrib Mineral Petrol 113:1–8

Hauri EH, Gaetani GA, Green TH (2004) Patitioning of H_2O between mantle minerals and silicate melts. Geochim Cosmochim Acta 68:A33

Hill E, Wood BJ, Blundy JD (2000) The effect of Ca-Tschermaks component on trace element partitioning between clinopyroxene and silicate melt. Lithos 53:203–215

Irving AJ, Frey FA (1984) Trace element abundances in megacrysts and their host rocks: Constraints on partition coefficients and megacryst genesis. Geochim Cosmochim Acta 48:1201–1221

Liotard JM, Briot D, Boivin P (1988) Petrological and geochemical relationships between pyroxene megacrysts and associated alkali-basalts from Massif Central (France). Contrib Mineral Petrol 98:81–90

Nielsen RL (1985) A method for the elimination of the compositional dependence of trace element distribution coefficients. Geochim Cosmochim Acta 49:1775–1779

Onuma N, Higuchi H, Wakita H, Nagasawa H (1968) Trace element partitioning between two pyroxenes and the host lava. Earth Planet Sci Lett 5:47–51

Pouchou JL, Pichoir F (1984) A new model for quantitative X-ray microanalysis, Part I. applications to the analysis of homogeneous samples. Rech Aerosp 3:13–38

Schosnig M, Hoffer E (1998) Compositional dependence of REE partitioning between diopside and melt at 1 atmosphere. Contrib Mineral Petrol 133:205–216

Sutherland FL, Hollis JD, Barron LM (1984) Garnet lherzolite and other inclusions from a basalt flow, Bow Hill, Tasmania. Proc 3rd Int Kimberlite Conf 2:145–160

van Westrenen W, Blundy JD, Wood BJ (1999) Crystal-chemical controls on trace element partitioning between garnet and anhydrous silicate melt

van Westrenen W, Allan NL, Blundy JD, Laurentieu L Yu, Lucas BR, Purton JA (2003a) Trace element incorporation into pyrope-grossular solid solutions, an atomistic simulation study. Phys Chem Minerals 30:217–229

van Westrenen W, Allan NL, Blundy JD, Laurentieu L Yu, Lucas BR, Purton JA (2003b) Dopant incorporation into garnet solid solutions—a breakdown of Goldschmidt's first rule. Chem Commun 6:786–787

Wood BJ, Blundy JD (2001) The effect of cation charge on crystal-melt partitioning of trace elements. Earth Planet Sci Lett 188:59–71

Wood BJ, Blundy JD (2002) The effect of H_2O on crystal-melt partitioning of trace elements. Geochim Cosmochim Acta 66:3647–3656

Xu X, O'Reilly SY, Griffin WL, Zhou X, Huang X (1998) The nature of the Cenozoic lithosphere at Nushan, eastern China. In: Flower M, Chung SL, Lo CH, Lee TY (eds) Mantle dynamics and plate interactions in East Asia. American Geophysical Union, Washington, DC, Geodynamics, vol 27. pp 167–196